



Supporting hierarchical soil biogeochemical modeling: Version 2 of the Biogeochemical Transport and Reaction model (BeTR-v2)

Jinyun Tang, William J. Riley, and Qing Zhu

Climate and Ecosystem Science Division, Lawrence Berkeley National Laboratory, Berkeley, CA, USA

5

Correspondence to: Jinyun Tang (jinyuntang@lbl.gov)

Abstract. Reliable soil biogeochemical modeling is a prerequisite for credible projections of climate change and associated ecosystem feedbacks. This recognition has called for frameworks that can support flexible and efficient development and application of new or alternative soil biogeochemical modules in earth system models (ESMs). The BeTR-v1 code (i.e., CLM4-BeTR) is one such framework designed to accelerate the development and integration of new soil biogeochemistry formulations into ESMs, and to analyze structural uncertainty in ESM simulations. With a generic reactive transport capability, BeTR-v1 can represent multi-phase (e.g., gaseous, aqueous, and solid), multi-tracer (e.g., nitrate and organic carbon), and multi-organism (e.g., plants, bacteria and fungi) dynamics. Here, we describe the new version BeTR-v2, which adopts more robust numerical algorithms and improves on structural design over BeTR-v1. BeTR-v2 better supports different mathematical formulations in a hierarchical manner by allowing the resultant model be run either for a single topsoil layer, a vertically resolved soil column, or fully coupled with the land component of the Energy Exascale Earth System Model (E3SM). We demonstrate the BeTR-v2 capability with benchmark cases and example soil BGC implementations. By taking advantage of BeTR-v2's generic structure integrated in E3SM, we then found that calibration could not resolve biases introduced by different numerical coupling strategies of plant-soil biogeochemistry. These results highlight the importance of numerically robust

10
15
20



implementation of soil biogeochemistry and coupling with hydrology, thermal dynamics, and plants—capabilities that the open-source BeTR-v2 provides.

1 Introduction

Soil biogeochemical (BGC) modeling is essential for predicting terrestrial ecosystem dynamics
5 in natural and managed lands, and is an important component of ESMs that perform projections and
hindcasts of ecosystem-climate feedbacks (e.g., Golaz et al., 2019; Hurrell et al., 2013). Over the years,
many soil BGC models have been developed, each of which has its merits and deficiencies (e.g., Zaehle
et al., 2014). Nonetheless, when the carbon dynamics simulated by many different ecosystem models
(including those integrated within ESMs) are synthesized, large uncertainties prevail (e.g., Davies-
10 Barnard et al., 2020; Todd-Brown et al., 2014). Several sources, including parametric, structural,
numerical, and boundary conditions (e.g., forcing and initial conditions), have been cited to explain the
large modeling uncertainty (Ahlstrom et al., 2013; Huntzinger et al., 2017; Tang and Riley, 2018).
Accordingly, various strategies have been proposed to alleviate or constrain these types of uncertainty
(Luo et al., 2012; Riley et al., 2021; Wieder et al., 2015; Zhu et al., 2019).

15 From the many uncertainty quantification studies, one urgent need identified is for a software
platform to support systematic comparisons of how different soil BGC formulations influence simulated
soil BGC feedbacks within a single ecosystem model, thereby facilitating more process-specific
hypotheses testing. To address this infrastructural gap, BeTR-v1 was developed as a submodule of the
community land model version 4 (CLM4; Tang et al., 2013). The design philosophy of BeTR is that,
20 assuming all else equal, one can investigate: (1) various levels of mechanistic complexity and model



formulations even for the same number of biogeochemical processes being represented, (2) the same mathematical formulation with different numerical method implementations (e.g., Tang and Riley, 2018), and (3) share of common process representations across diverse ecosystem types. For point (1), some researchers have argued that more explicit representation of processes are needed to resolve
5 complex soil BGC dynamics (Berardi et al., 2020; Riley et al., 2021; Tang and Riley, 2020; Wieder et al., 2015). For instance, active transport of various substrates in soils is needed if microbial dynamics are explicitly considered (e.g. Ahrens et al., 2015; Dwivedi et al., 2017; Grant, 2013; Riley et al., 2021). Point (2) is less discussed in land BGC modeling, but has been clearly called out in computational biology and computational geophysical fluids (e.g. Gross et al., 2018; Petrovskii and Petrovskaya,
10 2012). For point (3), aqueous environments, such as wetlands, groundwater, rivers, lakes and ocean, share many biogeochemical processes with soils, but different representations are often used (e.g., early diagenesis in marine sediments vs terrestrial soil organic matter decomposition; Koven et al., 2013; Munhoven, 2021). Therefore, developing a generic modeling infrastructure could benefit the mechanistic consistency in integrated earth system BGC modeling (e.g. Fisher and Koven, 2020).

15 Since the publication of BeTR-v1, we made a number of new developments in numerical algorithms for transport and BGC process coupling (Tang and Riley, 2016, 2014). We also made a better use of the object-oriented programming feature of Fortran 2003 to enable more efficient code sharing among the Fortran modules. All these are integrated into BeTR-v2: a platform to accelerate soil BGC model development and enable efficient code and knowledge share among ESM BGC
20 components. Below, we describe in detail the improvements that have brought into BeTR-v2 since BeTR-v1, give some examples based on its integration with the land module of E3SM (ELM; Burrows



et al., 2020), and then apply the model to evaluate whether parameter calibration can resolve the uncertainty associated with different numerical implementations.

2 Model developments

BeTR-v2 adopts the same governing equations as in BeTR-v1, but implements improved numerical algorithms (developed after the development of BeTR-v1) for both tracer transport and biogeochemical reaction coupling (to be described in section 2.1). Compared to BeTR-v1, BeTR-v2 is also better modularized and structured software-wise. Importantly, BeTR-v2 is a standalone capability to support more efficient model development and soil BGC coupling to alternative host models (E3SM in this case), while BeTR-v1 is embedded within CLM4.5 and cannot be run independently. It is noted that significant code re-writing and data restructuring have occurred since ELM branched out from CLM4.5, a comparison between BeTR-v1 and BeTR-v2 is not feasible.

2.1 Governing equations and numerical implementation

Same as BeTR-v1, BeTR-v2 solves the following one-dimensional reactive-transport equation

$$\begin{aligned} \frac{\partial}{\partial t} (\theta_w C_w + \varepsilon_g C_g + (1 - \theta_w - \varepsilon_g) C_s) \\ = \frac{\partial}{\partial z} \left(\theta_w \tau_w D_w \frac{\partial C_w}{\partial z} \right) + \frac{\partial}{\partial z} \left(\varepsilon_g \tau_g D_g \frac{\partial C_g}{\partial z} \right) \\ + \frac{\partial}{\partial z} \left((1 - \theta_w - \varepsilon_g) D_s \frac{\partial C_s}{\partial z} \right) - \frac{\partial}{\partial z} \left(q_w \frac{\partial C_w}{\partial z} \right) - E_{bub} - T_r \\ + R_{bgc} \end{aligned} \quad (1)$$

where θ_w is volumetric water content ($\text{m}^3 \text{m}^{-3}$), C_w is aqueous concentration (mol m^{-3}), ε_g is air-filled porosity ($\text{m}^3 \text{m}^{-3}$), C_g is gaseous concentration (mol m^{-3}), C_s is adsorbed concentration (mol m^{-3}), τ_w is aqueous tortuosity (unitless), τ_g is gaseous tortuosity (unitless), D_w is aqueous diffusivity ($\text{m}^2 \text{s}^{-1}$), D_g is gaseous diffusivity ($\text{m}^2 \text{s}^{-1}$), D_s is solid phase diffusivity ($\text{m}^2 \text{s}^{-1}$); as an approximation for processes like



bioturbation (Jarvis et al., 2010) and cryoturbation (Koven et al., 2009), which do not have mechanistically-based formulations), q_w is aqueous advection (m s^{-1}), E_{bub} is ebullition flux ($\text{mol m}^{-3} \text{s}^{-1}$), T_r is transport via transpiration flux ($\text{mol m}^{-3} \text{s}^{-1}$; including aerenchyma enabled gas transport), and R_{bgc} is biogeochemical reaction rate ($\text{mol m}^{-3} \text{s}^{-1}$).

5 Depending on how z (m) is interpreted, the transport can be regarded as either vertical or horizontal, provided that the advection velocity q_w is defined accordingly.

Besides the one-dimensional solution, BeTR-v2 also solves standalone single-layer models (a new feature that BeTR-v1 does not have), whose governing equation is

$$\frac{\partial}{\partial t} (\theta_w C_w + \varepsilon_g C_g + (1 - \theta_w - \varepsilon_g) C_s) = R_{bgc} + \frac{g_{as}}{\Delta z} (C_{atm} - C_g) \quad (2)$$

where g_{as} is the conductance (m s^{-1}) for the gaseous exchange of the tracer between soil and air, C_{atm} is the atmospheric gas concentration (mol m^{-3}), and Δz (m) is the single layer thickness (taken as 10 cm in the examples below). Simulations from equation (2) can be used to compare with incubation experiments.

To achieve numerically robust solutions and to adapt to the hydrological dynamics in ELM (which solves surface runoff, variably saturated flow, and subsurface drainage sequentially), equation (1) is solved with the operator splitting approach (Simpson and Landman, 2007). Specifically, tracer loss through surface runoff is solved first, then biogeochemical reactions are solved, followed by advection, diffusion, ebullition (using the hydrostatic approximation from Tang et al. (2010)), and subsurface drainage. For diffusion, gaseous and aqueous diffusion are solved together using the implicit dual-phase algorithm with the implicit time stepping method (Tang and Riley, 2014), which is equally



accurate but simpler than the treatment in BeTR-v1 that requires the information of wetting fronts in soil. Solid phase diffusion is also solved implicitly. Aqueous advection is solved using the mass-conserving semi-Lagrangian approach (Manson and Wallis, 2000), which is more accurate than the upstream scheme used in BeTR-v1.

5 2.2 Code structure

The open-source BeTR-v2 code can be found at <https://github.com/BeTR-biogeochemistry-modeling/sbetr/tree/jinyuntang/ELM-BeTR-ECA.r> (and it is also archived at <https://doi.org/10.5281/zenodo.5526854>), where each folder has a readme.md file explaining the purpose of each sub-directory or each source code file. For interested users, the major code to look into

10 is under the directories “sbetr/src/betr” (core betr code), “sbetr/src/Applications” (customized BGC modules), “sbetr/src/driver/” (driver files for 1D models and APIs to couple BeTR with land models like ELM), and “sbetr/src/jarmodel/” (driver files for single layer models). In the directory “src/Applications/soil-farm”, each folder (except “bgcfarm_util”) is a soil BGC implementation. For this manuscript, the BGC implementation ELMv1-BeTR-ECA under the directory

15 “sbetr/src/Applications/soil-farm/v1eca/” is used to test the global simulation capability of BeTR, while *ecacnp* under “sbetr/src/Applications/soil-farm/ecacnp/” is used to demonstrate the standalone simulation capability. More details about why two implementations are used for different purposes will be explained in section 2.4. Instructions on how to build and run BeTR on typical platforms can be found at <https://github.com/BeTR-biogeochemistry-modeling/sbetr>.

20 2.3 Model benchmark and verification



As we did for BeTR-v1, two analytical solutions to equation (3) with different boundary

conditions are employed to benchmark the numerical accuracy of the BeTR-v2 reactive transport solver:

$$\frac{\partial C}{\partial t} = \frac{\partial}{\partial z} \left(D \frac{\partial C}{\partial z} \right) - u \frac{\partial C}{\partial z} \quad (3)$$

where D ($\text{m}^2 \text{s}^{-1}$) and u (m s^{-1}) are diffusivity and advection velocity, respectively.

The two analytical solutions are

$$C = \frac{1}{2} \operatorname{erfc} \left(\frac{z - ut}{2\sqrt{Dt}} \right) + \frac{1}{2} \exp \left(\frac{uz}{D} \right) \operatorname{erfc} \left(\frac{z + ut}{2\sqrt{Dt}} \right) + \left[1 + \frac{u}{2D} (2L - z + ut) \right] \\ \times \exp \left(\frac{uL}{D} \right) \operatorname{erfc} \left(\frac{2L - z + ut}{2\sqrt{Dt}} \right) - \sqrt{\frac{u^2 t}{\pi D}} \exp \left[\frac{uL}{D} - \frac{(2L - z + ut)^2}{4Dt} \right] \quad (4)$$

5 for a pulse tracer imposed at the top of a 1-D soil column of length L (Kumar et al., 2009), where $\operatorname{erfc}(x)$ is the complementary error function of x ; and

$$C = C_0 + \sum_{i=1}^2 A_i \exp \left(-\frac{u}{2D} - \frac{\sqrt{2}z}{4D} \sqrt{u^2 + \sqrt{u^4 + 16D^2\omega_i^2}} \right) \\ \times \sin \left(\omega_i t - \frac{\sqrt{2}\omega_i z}{\sqrt{u^2 + \sqrt{u^4 + 16D^2\omega_i^2}}} \right) \quad (5)$$

for a wave-like tracer imposed at the top of a 1-D soil column, where $C_0 = 12/23 \text{ mol tracer m}^{-3}$, $A_1 = 9/23 \text{ mol tracer m}^{-3}$, $A_2 = 2/23 \text{ mol tracer m}^{-3}$, $\omega_1 = 2\pi/365 \text{ day}^{-1}$ and $\omega_2 = 2\pi \text{ day}^{-1}$. For both cases, $u = 10^{-7} \text{ m s}^{-1}$, $D = 1.3 \times 10^{-6} \text{ m}^2 \text{ s}^{-1}$, and $L = 35.17 \text{ m}$, and the lower boundary condition is

$$\frac{\partial C}{\partial t} + u \frac{\partial C}{\partial z} = 0 \quad (6)$$

10 These two tests have been integrated as part of the standard test suit for BeTR-v2. After doing “make test” by following the instructions, their output can be found under “regression-tests/tests/standalone/” as analytical-adr-b1 and analytical-adr-b2, respectively.



2.4 Example soil BGC implementation

We re-implemented the soil BGC from ELMv1-ECA (Zhu et al., 2019) to illustrate the capability of BeTR-v2. By re-implementation we mean to solve the ELMv1-ECA soil BGC in the form of equation (1) in BeTR-v2 based on input fluxes of organic matter and nutrients from ELM and return
5 fluxes of carbon and nutrient fluxes to ELM (after calculations in BeTR-v2). The ELMv1-ECA soil BGC model consists of a Century-like soil carbon decomposition cascade based on Koven et al. (2013), but competition of inorganic nitrogen (ammonium and nitrate) and phosphorus between plants and (the implicitly represented) microbial organisms is calculated using the Equilibrium Chemistry Approximation kinetics (Tang and Riley, 2013; Zhu et al., 2016). The performance of ELMv1-ECA
10 was evaluated comprehensively by using the International Land Model Benchmarking (ILAMB) system (Collier et al., 2018; Zhu et al., 2019). Differing from other nutrient competition paradigms, particularly the popular relative demand approach that is implemented in many existing BGC models (Riley et al., 2018), the ECA approach explicitly considers the kinetic traits of the involved plants, microbes, and soil sorption surfaces, and is more capable of resolving the diverse dynamical processes involved in plant-
15 soil nutrient competition (Medvigy et al., 2019; Tang and Riley, 2021; Zhu et al., 2017).

In BeTR-v2, a soil BGC formulation is implemented in two-steps: (1) a single-layer implementation of the given soil BGC process, which is then populated through BeTR-v2's reactive transport code to form (2) a 1-D vertically resolved implementation of the soil BGC process. Take *ecacnp* for example, the single-layer implementation is in the folder “*ecacnp/ecacnp1layer/*”, which is
20 extended to 1-D soil column using codes in the folder “*ecacnp/ecacnpNlayer/*”, and corresponding model parameters are set using codes in the folder “*ecacnp/ecacnpPara/*”. The single-layer code is called



by the driver file in “sbetr/src/jarmodel/driver” to conduct single layer simulations. (In contrast, BeTR-v1 did not separate the single-layer models from the vertically resolved models.) The soil BGC formulations in the folder “src/Applications/soil-farm/ecacnp” adopts the mathematical formulation of the soil BGC module from ELMv1-ECA, but concurrently solves the incoming litter input, soil carbon decomposition, nitrification-denitrification, plant-soil nutrient competition, etc. when updating the soil BGC state variables. The treatment in *ecacnp* enables us to cleanly separate vegetation and soil BGC in ELM, but requires a significant amount of reordering of the subroutines and two additional parameters for plant BGC. That is, besides the introduction of two parameters on the turnover of plant nitrogen and phosphorus storage pools, *ecacnp* has to compute soil BGC and plant-soil nutrient competition after all the phenological updates (including plant carbon and nutrient allocation for growth and vegetation mortality induced by fire and other natural factors), whereas ELMv1-ECA computes plant-soil nutrient competition before updating the phenological variables. When using the same parameters, the reordering required by *ecacnp* caused significant differences in the simulated carbon and nutrient cycling compared to ELMv1-ECA, and such differences were inferred not to be easily correctable by calibration, confirming our previous findings (based on BeTR-v1) in Tang and Riley (2018). Therefore, we did another implementation of the soil BGC of ELMv1-ECA in BeTR-v2 by following the exact subroutine execution order of ELMv1-ECA, and named it as ECAv1-BeTR-ECA0 (code is in src/Applications/soil-farm/v1eca). ELMv1-BeTR-ECA0 can run with the same parameters as those in ELMv1-ECA, thus minimizing the need to change parameters to obtain acceptable simulations. Since we found that ELMv1-BeTR-ECA0 performed significantly different from ELMv1-ECA, we include



ELMv1-BeTR-ECA by calibrating $vIeca$ against ELMv1-ECA to evaluate to what extent the model behavior differences can be reduced by adjusting model parameters.

Overall, ELMv1-BeTR-ECA0 differs from ELMv1-ECA in two aspects: (1) in belowground BGC, ELMv1-BeTR-ECA0 solves the plant-soil nutrient competition using the multiple-flux-co-limiting solver, such that nutrient mineralization and immobilization are concurrently coupled (Tang and Riley, 2016), whereas ELMv1-ECA solves nutrient mineralization and uptake asynchronously using the explicit Euler scheme, where newly mineralized nutrients at the current time step become available only in the next time step, and (2) for aboveground BGC, ELMv1-BeTR-ECA0 solves plant carbon and nutrient allocation for growth using the multiple-flux-co-limiting solver to avoid sporadic negative litter flux inputs to the soil BGC, whereas ELMv1-ECA updates these state variable sequentially using the explicit Euler scheme and only corrects negative variables (which occur sporadically) at the end of each simulation step. ELMv1-BeTR-ECA differs from ELMv1-BeTR-ECA0 with values of the model parameters. Besides these three configurations, we also included ELMv1-ECA-V that differs from ELMv1-ECA by using the multiple-flux-co-limiting solver for plant carbon and nutrient allocation. A brief description of the four model configurations is in Table 1.

All in all, by using *ecacnp* soil BGC for standalone simulations (which can be created by following the instructions in the frontpage of sbetr git repo), we demonstrate how BeTR-v2 can support an easy extension from a single-layer model to a 1-D vertically-resolved model. Comparing ELMv1-ECA and ELMv1-ECA, we verify the correct implementation of the multiple-flux-co-limiting solver. Using ELMv1-BeTR-ECA0 for ELM-coupled simulations, we demonstrate that different numerical implementations for the same BGC formulation results in significantly different model behavior. More



importantly, by using ELMv1-BeTR-ECA we also show that such model behavior differences cannot be resolved by recalibrating model parameters.

We drove the standalone 1D model simulation with 365-day half-hourly time step output from an earlier ELM simulation Zhu et al. (2019). Model input variables include vertically resolved litter
5 fluxes (of carbon, nitrogen and phosphorus), soil temperature and moisture, infiltration flux, and atmospheric pressure and temperature. The example simulations are from the CA-Gro Ameriflux site: Ontario-Groundhog River, Boreal Mixedwood Forest (see <http://sites.fluxdata.org/CA-Gro/> for more descriptions of the site). The single layer simulation used inputs for the first soil layer. For all global
10 al., 2019), and a transient simulation from 1850-2010. All forcing data are the same from Zhu et al. (2019), and all simulations are 1.9° latitude by 2.5° longitude spatial resolution.

Table 1. Summary of the configurations for the four global simulations.

| Model configuration | Short description |
|---------------------|--|
| ELMv1-ECA | Default ELMv1-ECA |
| ELMv1-ECA-V | Same as ELMv1-ECA, but used the multiple-flux-co-limiting solver for plant carbon and nutrient allocation. |
| ELMv1-BeTR-ECA0 | Based on src/Applications/soil-farm/v1eca, and used the multiple-flux-co-limiting solver for plant carbon and nutrient allocation. |
| ELMv1-BeTR-ECA | Using the same code as did ELMv1-BeTR-ECA0, but recalibrated two tropical plant functional types against ELMv1-ECA. |



3 Results

3.1 Benchmark of the BeTR-v2 transport code

We found that the BeTR-v2 advection-diffusion solver solutions agreed well with the analytical solutions for both benchmarking cases (Figure 1). For the pulse tracer solution (left panels in Figure 1),
5 the depth-averaged root mean square error (RMSE) and R^2 of linear fitting are 0.013 mol m^{-3} and 0.999, respectively, and for the wave-like solution (right panels in Figure 1), these two metrics are $0.0050 \text{ mol m}^{-3}$ and 0.999, respectively. As time increases, we observed some increase in the RMSE for both benchmark cases, however, the overall magnitudes are still small (Figure 1e, f). Overall, we infer that using the exponential spatial discretization from ELM (which is similar to that in CLM (Oleson et al.,
10 2013)) for the BeTR-v2 solver led to very accurate reproduction of the analytical solutions.

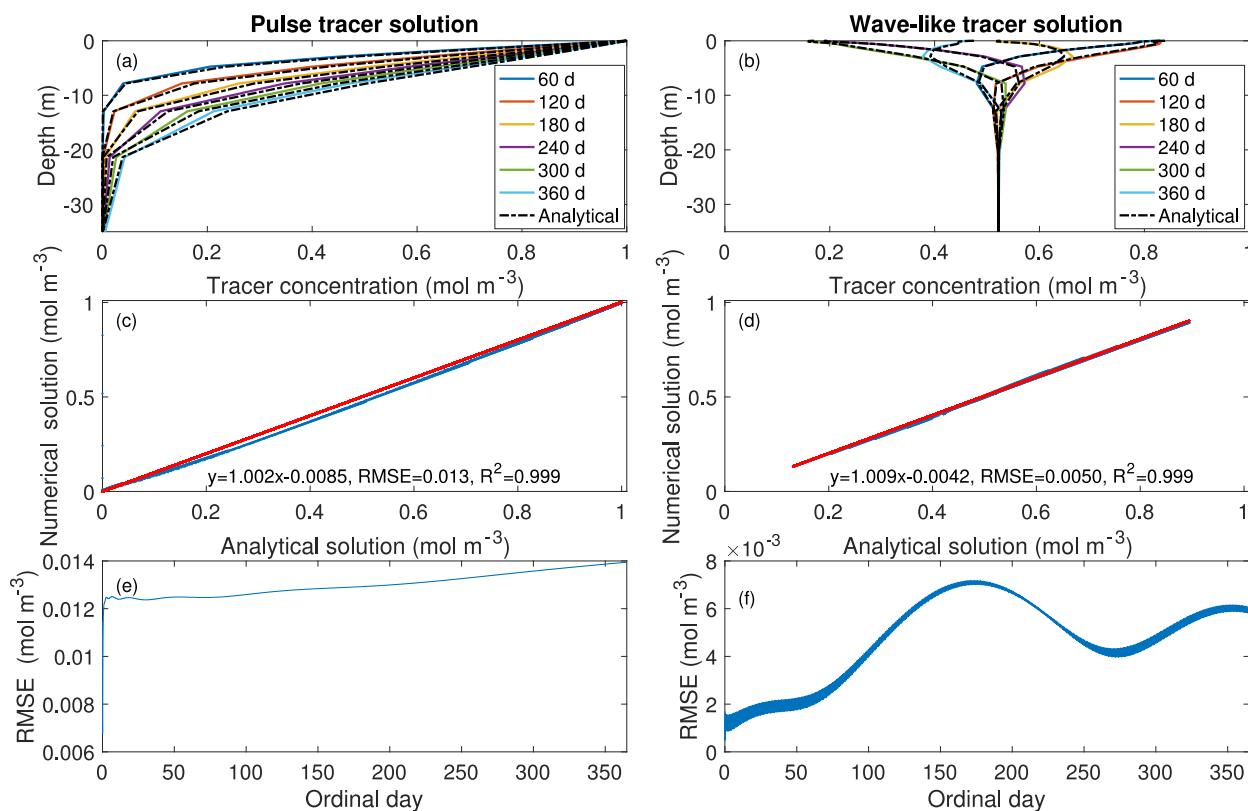


Figure 1. Comparison of the analytical solutions to the numerical solutions derived from BeTR-v2. (a) and (b) are comparisons of simulated and analytical tracer concentrations sampled at the end of 6 different days. In panels (c) and (d), blue dots are plotted using analytical solutions as x axis and numerical solutions as y axis; red lines are linear regressions of these data. Panels (e) and (f) are the depth-averaged root mean square error (RMSE) through time.



3.2 Single-layer and 1D column model simulations

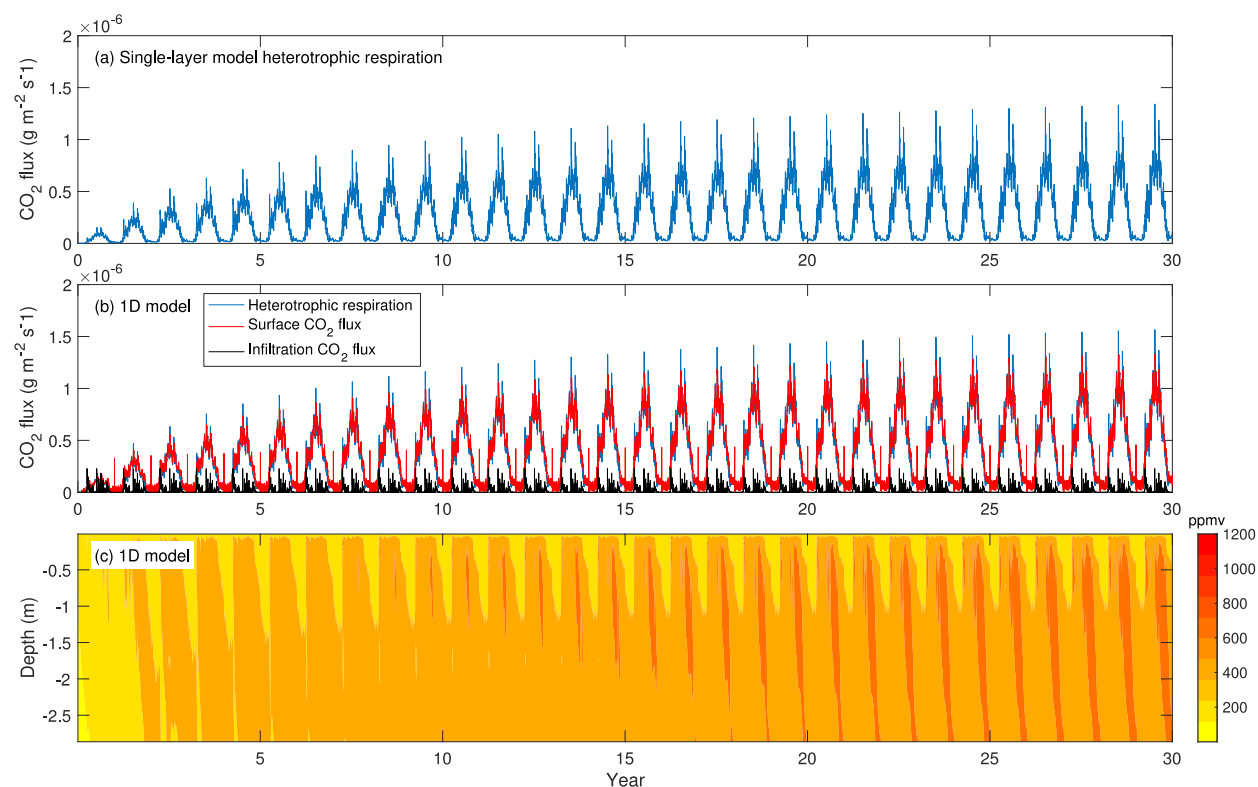


Figure 2 (a) Heterotrophic CO₂ flux simulated by the 10-cm thick single layer model; (b) column
integrated heterotrophic flux, soil surface CO₂ flux and CO₂ infiltration flux; (c) evolution of soil CO₂
concentration corresponding to panel (b). The single layer model used the forcing data for the first layer
of the 10-layer model.

In the example standalone simulations using the *ecacnp* soil BGC, the single-layer and the
vertically-resolved 10-layer models demonstrate very similar temporal patterns for heterotrophic CO₂
production (Figure 2a and Figure 2b). For the 1D vertically-resolved model simulation, surface CO₂
flux is smaller than the heterotrophic CO₂ respiration plus infiltration CO₂ flux throughout the 30-year
period. Accordingly, the soil CO₂ concentration builds up continuously, with a seasonal cycle that has
its maximum in July and minimum in March. (We did not run the 1D model to equilibrium, because the



example case here is only used for demonstration and to check if the model behavior agrees with our physical intuition. Additionally, this example does not account for root respiration. Therefore, we do not expect the soil CO₂ to be as high as 10000 ppm as it is often observed (Hirano et al., 2003), although in global simulations, we do find soil CO₂ below 30 cm could reach as high as a few percent.) In a
5 previous study with BeTR-v1 (Tang et al., 2013), we showed that some water-dissolved soil CO₂ can be lost through the hydrological outflow. However, this hydrological loss is small in the above simulation because the forcing data does not include lateral runoff (i.e., lateral runoff is set to zero for standalone simulations for simplicity), and the leaching is negligible. Overall, we conclude that BeTR-v2 consistently represents vertically-resolved soil BGC reactions and transport.

10

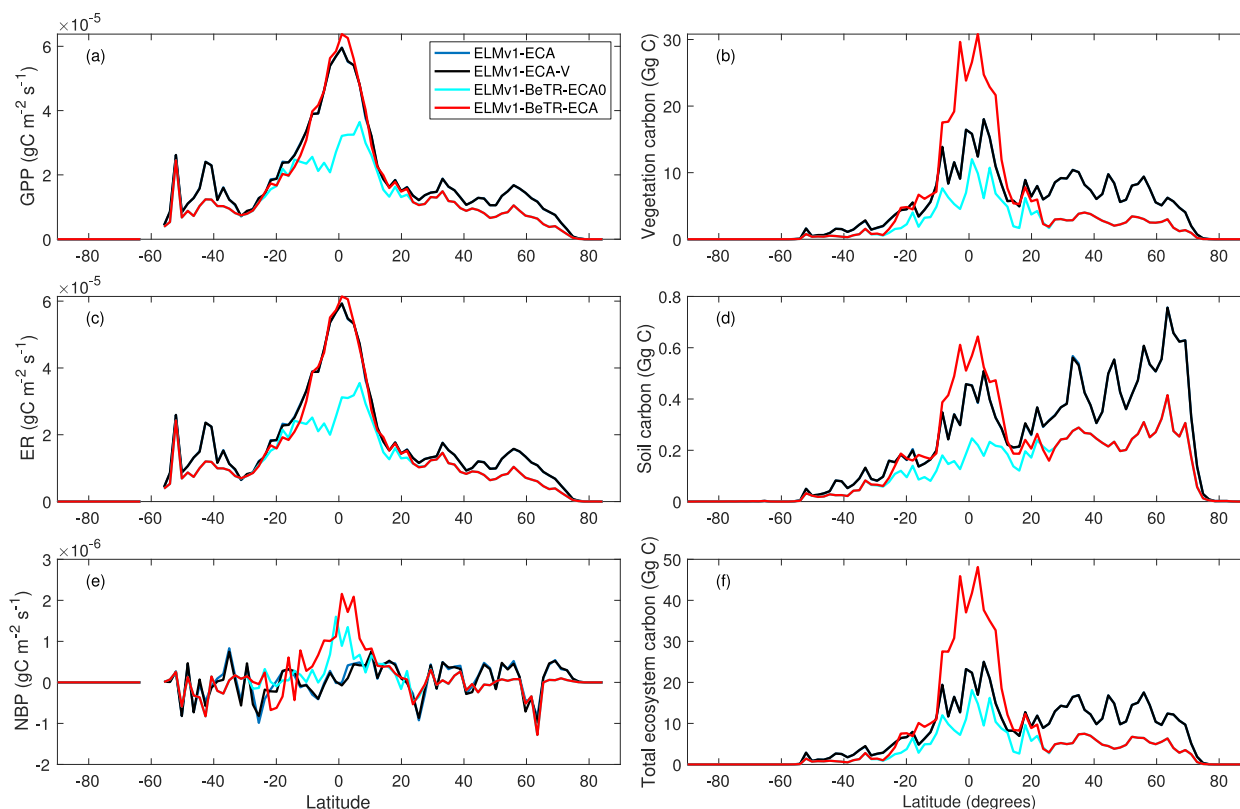


Figure 3. Comparison of simulated flux and state variables at the end of 200th year during the accelerated spinup for four model configurations (see Table 1). ELMv1-ECA-V differs from ELMv1-ECA by using the multiple-flux-co-limiting solver for allocating carbon and nutrient for plant growth. ELMv1-BeTR-ECA0 differs from ELMv1-ECA-V by further solving belowground nutrient competition using the multiple-flux-co-limiting solver. ELMv1-BeTR-ECA differs from ELMv1-BeTR-ECA0 by using re-calibrated parameters for two tropical plant functional types: broad leaf evergreen tropical tree and broadleaf deciduous tropical tree. We note that the soil carbon here is smaller than vegetation carbon because factors of accelerated decomposition have not been applied.

3.3 Global simulations

We first ran three global model configurations for a 200-year accelerated spinup using the same parameters (see Koven et al. (2013) for information on how accelerated spinup is designed). Because there was very little competition among the plant organs for carbon and nutrients, the spinup simulations led to almost identical model outputs between ELMv1-ECA and ELMv1-ECA-V (Figure



3), suggesting that resolved plant carbon and nutrient allocation using the multiple-flux-co-limiting solver has negligible influence and this solver is properly implemented. ELMv1-BeTR-ECA0 (cyan lines) and ELMv1-ECA (blue lines) produced very different latitudinal patterns of primary flux variables, such as GPP (gross primary productivity; Figure 3a) and ER (ecosystem respiration; Figure 5 3c), and therefore NBP (net biome productivity; Figure 3e), particularly in the tropics. Noticeable differences among fluxes are also found in the middle to high latitudes. Accordingly, the vegetation, soil, and total ecosystem carbon pools differ substantially between ELMv1-ECA and ELMv1-BeTR-ECA0 (Figure 3b, d, f) in the tropics and northern middle to high latitudes. We found that the differences were caused by different nutrient uptake rates simulated by the two models. In particular, 10 with the multiple-flux-co-limiting solver, both plants and soil carbon processes in ELMv1-BeTR-ECA0 were overall less nitrogen limited given the same nutrient uptake parameters, but as the simulation proceeded in time, less soil carbon was accumulated and soils became less fertile, consistent with our previous finding (Tang and Riley, 2018).

Since the simulated differences between ELMv1-BeTR-ECA0 and ELMv1-ECA are caused by 15 different numerical implementations and are greatest in the tropics, we calibrated ELMv1-BeTR-ECA0 with respect to ELMv1-ECA for plant parameters important for plant-soil coupling for two tropical plant functional types (Table 2) and to analyze to what extent these differences can be minimized. (We spared the other plant function types because including them in calibration is unlikely to change the conclusion of our analysis, as we will see later, while this decision significantly reduced the carbon 20 footprint of this computationally intensive study.) We conducted the parameter calibration using predicted total-column soil C, vegetation C, GPP, ER, and leaf area index from ELMv1-ECA as



constraints. We applied the grid-search approach (e.g., Bergstra and Bengio, 2012) to iteratively minimize model differences until no significant further improvement could be obtained. (We ended up with 10 iterations where each iteration consists of 50 simulations.)

We found significant differences between default and calibrated model parameter values (Table 2). For ELMv1-BeTR-ECA, the calibrated substrate affinity parameters for NH_4^+ and NO_3^- are of the same magnitudes as their default counterparts. The maximum uptake rates for NH_4^+ and NO_3^- and the maximum nitrogen fixation rates are of the same order as their default values. For both PFT-4 and PFT-6, a higher amount of fixed nitrogen is directly acquired by plants in ELMv1-BeTR-ECA. When these new parameters were accordingly applied to tropical grid cells, we found smaller differences between ELMv1-ECA and ELMv1-BeTR-ECA for GPP and ER in the tropics (Figure 3a and Figure 3c), while differences in other variables remain quite significant (Figure 3). Therefore, we assert that different numerical implementations result in different model predictions, and such different model predictions are unlikely to be rectified by parameter calibration.

Table 2. Comparison of calibrated (ELMv1-BeTR-ECA) with default (ELMv1-ECA) parameters. PFT-4 is broad leaf evergreen tropical tree and PFT-6 is broadleaf deciduous tropical tree.

| Parameters | ELMv1- ECA | | ELMv1-ECA | |
|---|------------|----------|-----------|----------|
| | PFT-4 | PFT-6 | PFT-4 | PFT-6 |
| Maximum nitrogen fixation rate (s^{-1}) | 1.55e-09 | 4.06e-09 | 2.45e-09 | 6.55e-09 |
| Plant affinity for soil NH_4^+ (gN m^{-3}) | 0.14 | 0.14 | 0.18 | 0.24 |
| Plant affinity for soil NO_3^- (gN m^{-3}) | 0.27 | 0.27 | 0.31 | 0.17 |
| Maximum plant uptake rate for NH_4^+ (s^{-1}) | 5.11e-06 | 1.49e-08 | 2.83e-06 | 1.80e-08 |
| Maximum plant uptake rate for NO_3^- (s^{-1}) | 5.24e-07 | 1.60e-08 | 4.80e-07 | 1.58e-08 |
| Fixed N_2 Fraction directly entering plant | 0.8 | 0.5 | 0.85 | 0.75 |

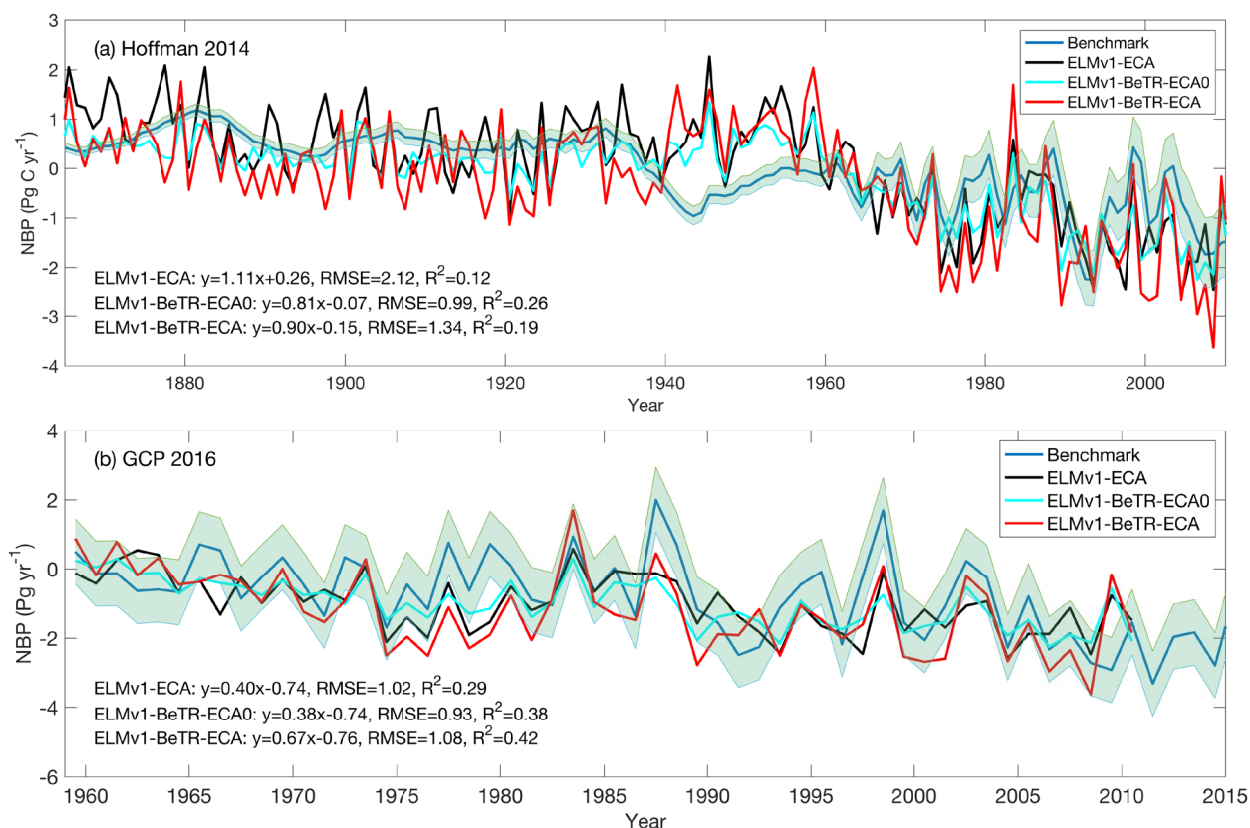


To further quantify the modeling uncertainty induced by different numerical implementations, we evaluated the four global simulations using the ILAMB benchmark software (Collier et al., 2018; version 2.5). Consistent with the results shown in Figure 3, ELMv1-ECA and ELMv1-ECA-V have almost identical performance (Table 3). ELMv1-BeTR-ECA0 performed similarly or worse than ELMv1-ECA, but significantly better for the metric of Global Net Ecosystem Carbon Balance (aka Net Biome Production, NBP, also see Figure 4). Out of eight carbon metrics, ELMv1-BeTR-ECA performed slightly worse than ELMv1-ECA in net ecosystem exchange, and significantly worse in vegetation biomass. For the remaining four hydrological cycle metrics, five radiation and energy metrics, and four climate forcing metrics, their performances are almost the same. ELMv1-BeTR-ECA performed slightly better for the metric of Global Net Ecosystem Carbon Balance (also see Figure 4). For functional-relationship benchmarks, ELMv1-BeTR-ECA0, ELMv1-BeTR-ECA and ELMv1-ECA performed quite similarly (Figure 5). Notably, ELMv1-BeTR-ECA was able to simulate higher evapotranspiration, resulting in better performance for the functional relationship between GPP and evapotranspiration (red line in Figure 5a). ELMv1-BeTR-ECA also performed slightly better in some cases, e.g., GPP vs. precipitation (Figure 5b), evapotranspiration vs. precipitation (Figure 5d), and leaf area index vs. precipitation (Figure 5e). This better agreement between ELMv1-BeTR-ECA and some benchmarks suggests that the numerical difference can indeed degrade the performance of a supposedly good mathematical representations of ecosystem biogeochemistry.

Nevertheless, there exist significant differences in the simulated nutrient dynamics (as reflected in the fast variables that have a significant seasonal cycle), which over a longer time period can affect the cumulative carbon state variables (e.g., right panels in Figure 3). For instance, for simulation year 2010,



the hydrological nitrogen loss estimated by ELMv1-ECA is $56.8 \text{ TgN year}^{-1}$, while that by ELMv1-BeTR-ECA is ~ 10 times smaller ($4.2 \text{ TgN year}^{-1}$; the value by ELMv1-BeTR-ECA0 is $4.5 \text{ TgN year}^{-1}$). The global N_2O emission estimated by ELMv1-ECA is $13.2 \text{ TgN year}^{-1}$, whereas ELMv1-BeTR-ECA estimated as $14.3 \text{ TgN year}^{-1}$ (and the value by ELMv1-BeTR-ECA0 is $12.5 \text{ TgN year}^{-1}$).



5

Figure 4. Benchmark of simulated NBP with two global syntheses. (a) Comparison with data from Hoffman et al. (2014); (b) Comparison with data from Le Quere et al. (2016). In the linear regression, x is benchmark, and y is model output.

10 Further, ELMv1-ECA and ELMv1-BeTR-ECA predicted different spatial distributions of plant nutrient limitations. For example, for simulation year 2010, ELMv1-ECA predicted higher nitrogen limitation to plant productivity in northern high-latitude regions and some regions in northwest Australia (Figure 6e), even though the general patterns of plant nitrogen limitation are very similar



(Figure 6a, b). However, compared to ELMv1-BeTR-ECA, ELMv1-ECA predicted much more widespread plant phosphorus limitation (Figure 6f). Therefore, a model calibration using carbon cycle variables led to very different estimates of N cycle parameters and thereby nitrogen dynamics. This type of discrepancy indicates that simulations under future climate with these two seemingly-similar models may very well diverge.

Table 3. Comparison of ILAMB scores for 23 simulated variables by three different model versions. The three entries in grey for ELMv1-BeTR-ECA (and ELMv1-BeTR-ECA0) differ by greater than 5% from ELMv1-ECA.

| Variables | ILAMB Scores | | | |
|-------------------------------------|----------------|-----------------|-----------|-------------|
| | ELMv1-BeTR-ECA | ELMv1-BeTR-ECA0 | ELMv1-ECA | ELMv1-ECA-V |
| Biomass | 0.466 | 0.494 | 0.642 | 0.642 |
| Carbon Dioxide | 0.730 | 0.685 | 0.688 | 0.690 |
| Gross Primary Productivity | 0.610 | 0.583 | 0.603 | 0.603 |
| Leaf Area Index | 0.536 | 0.520 | 0.540 | 0.541 |
| Global Net Ecosystem Carbon Balance | 0.789 | 0.817 | 0.626 | 0.626 |
| Net Ecosystem Exchange | 0.453 | 0.453 | 0.494 | 0.494 |
| Ecosystem Respiration | 0.577 | 0.573 | 0.576 | 0.576 |
| Soil Carbon | 0.699 | 0.698 | 0.713 | 0.713 |
| Evapotranspiration | 0.689 | 0.667 | 0.678 | 0.678 |
| Latent Heat | 0.682 | 0.703 | 0.688 | 0.688 |
| Sensible Heat | 0.634 | 0.684 | 0.638 | 0.638 |
| Terrestrial Water Storage Anomaly | 0.634 | 0.627 | 0.638 | 0.638 |
| Surface Upward SW Radiation | 0.639 | 0.639 | 0.644 | 0.644 |
| Surface Net SW Radiation | 0.798 | 0.797 | 0.799 | 0.799 |
| Surface Upward LW Radiation | 0.780 | 0.778 | 0.782 | 0.782 |
| Surface Net LW Radiation | 0.634 | 0.631 | 0.637 | 0.638 |
| Surface Net Radiation | 0.750 | 0.748 | 0.751 | 0.752 |
| Surface Air Temperature | 0.892 | 0.891 | 0.892 | 0.892 |
| Precipitation | 0.798 | 0.798 | 0.798 | 0.798 |
| Surface Downward SW Radiation | 0.857 | 0.857 | 0.857 | 0.857 |
| Surface Downward LW Radiation | 0.832 | 0.832 | 0.832 | 0.832 |

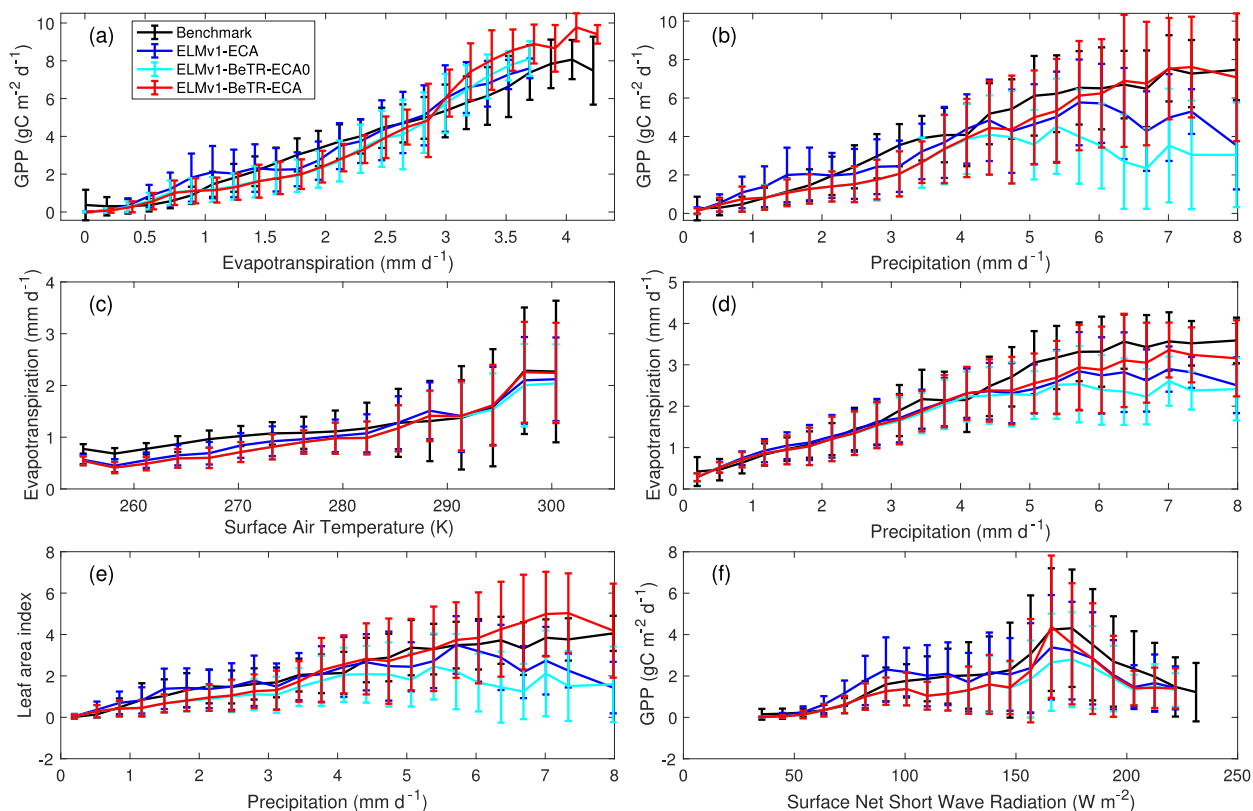


Figure 5. Benchmark of simulated vs. empirical data derived variable relationships. The empirical benchmarks are derived from FluxCom output for the period from January 1980 through December 2013 (Jung et al., 2017; Tramontana et al., 2016) and used in ILAMB.

5

In summary, adopting different numerical coupling strategies resulted in different model behavior, even with many similar carbon cycle metrics. In particular, we found important differences in N and P dynamics which could impact 21st century simulations when atmospheric CO₂ increases are expected to cause progressive nutrient limitations.

10

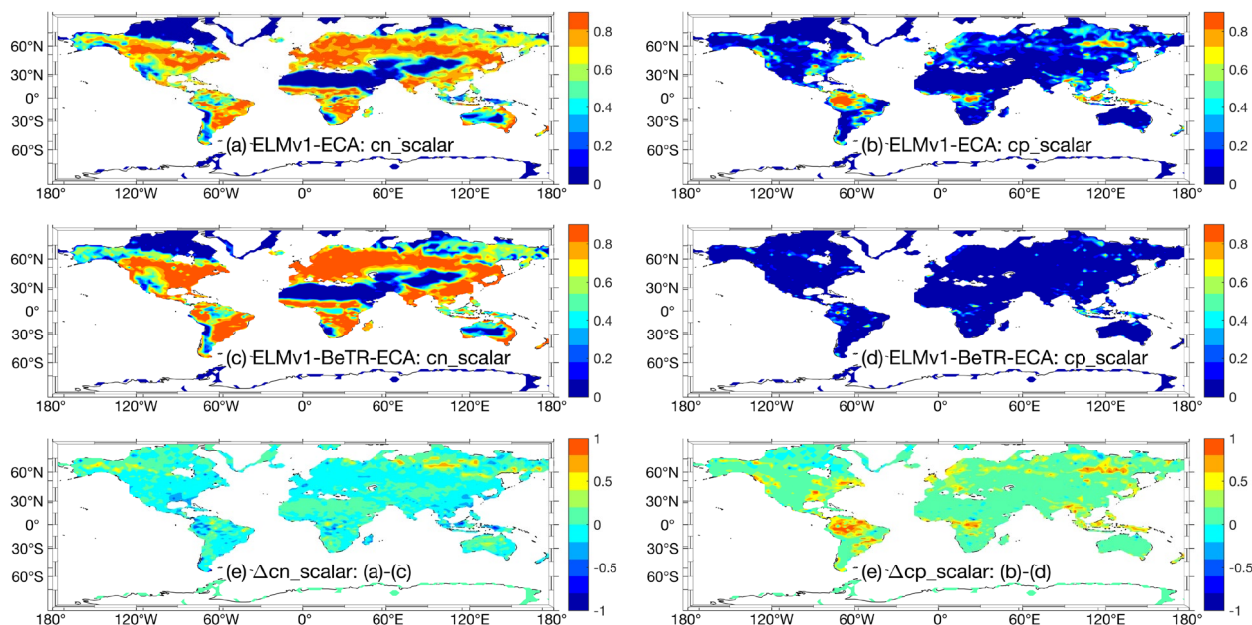


Figure 6. Comparison of simulated plant nutrient stresses (on the scale from zero to one) at year 2010. Left panels are for nitrogen stress and right panels are for phosphorus stress. Greater values indicate stronger limitation for the corresponding nutrient.

5 4. Conclusion

In this study, we present BeTR-v2, a reactive transport module for flexible implementation of soil biogeochemistry in ecosystem models. We benchmarked the numerical solver with two analytical solutions, and demonstrated that BeTR-v2 can support soil biogeochemical modeling in single-layer, 1D vertically-resolved single column, and global simulation modes. We implemented the soil biogeochemistry formulation from ELMv1-ECA into ELMv1-BeTR-ECA and explored the role of numerical solver robustness and calibration on carbon and nutrient cycling. We found that because the multiple-flux-limiter numerical solver (which is numerically more robust than the default ELMv1-ECA model; Tang and Riley (2018, 2016)) more tightly couples plant and soil processes during nutrient competition, ELMv1-BeTR-ECA has to use different model parameters to produce similar model behavior for carbon and water cycling. However, the calibration was not able to correct the important



differences in predicted N and P cycling, indicating that inappropriate numerical coupling can result in incorrect model parameters that may affect predictions of carbon cycling variables under a changing climate and increasing atmospheric CO₂ concentrations.

5 Code and data availability

For this study, BeTR-v2 can be accessed at <https://github.com/BeTR-biogeochemistry-modeling/sbetr/tree/jinyuntang/ELM-BeTR-ECA.r>, and is archived at

<https://doi.org/10.5281/zenodo.5526854>. ELM can be accessed at https://github.com/E3SM-Project/E3SM/tree/jinyuntang/lnd/betr_v2eca_qz_fix. ILAMB can be accessed at

10 <https://github.com/rubisco-sfa/ILAMB>. Model simulation data are available upon request from the first author, or be reproduced with the above codes and parameters in Table 2.

Author contributions

JYT developed the BeTR-v2 code and performed all model simulations. JYT, WJR and QZ did the model analysis and wrote the paper.

15 Competing interests

The authors declare no conflict of interest.

Acknowledgements

This research was supported by the Reducing Uncertainties in Biogeochemical Interactions through Synthesis and Computation (RUBISCO) Scientific Focus Area and the Energy Exascale Earth System

20 Modeling Project, which are sponsored by the Earth and Environmental Systems Modeling (EESM)

Program under the Office of Biological and Environmental Research of the US Department of Energy



Office of Science. Lawrence Berkeley National Laboratory (LBNL) is managed by the University of California for the US Department of Energy under Contract No. DE-AC02-05CH11231.

References

- Ahlstrom, A., Smith, B., Lindstrom, J., Rummukainen, M., and Uvo, C. B.: GCM characteristics explain the majority of uncertainty in projected 21st century terrestrial ecosystem carbon balance, *Biogeosciences*, 10, 1517-1528, 2013.
- Ahrens, B., Braakhekke, M. C., Guggenberger, G., Schrumpf, M., and Reichstein, M.: Contribution of sorption, DOC transport and microbial interactions to the C-14 age of a soil organic carbon profile: Insights from a calibrated process model, *Soil Biol Biochem*, 88, 390-402, 2015.
- 10 Berardi, D., Brzostek, E., Blanc-Betes, E., Davison, B., DeLucia, E. H., Hartman, M. D., Kent, J., Parton, W. J., Saha, D., and Hudiburg, T. W.: 21st-century biogeochemical modeling: Challenges for Century-based models and where do we go from here?, *GCB Bioenergy*, doi: 10.1111/gcbb.12730, 2020. 1-15, 2020.
- Bergstra, J. and Bengio, Y.: Random Search for Hyper-Parameter Optimization, *J Mach Learn Res*, 13, 15 281-305, 2012.
- Burrows, S. M., Maltrud, M., Yang, X., Zhu, Q., Jeffery, N., Shi, X., Ricciuto, D., Wang, S., Bisht, G., Tang, J., Wolfe, J., Harrop, B. E., Singh, B., Brent, L., Baldwin, S., Zhou, T., Cameron-Smith, P., Keen, N., Collier, N., Xu, M., Hunke, E. C., Elliott, S. M., Turner, A. K., Li, H., Wang, H., Golaz, J. C., Bond-Lamberty, B., Hoffman, F. M., Riley, W. J., Thornton, P. E., Calvin, K., and Leung, L. R.: The DOE 20 E3SM v1.1 Biogeochemistry Configuration: Description and Simulated Ecosystem-Climatic Responses to Historical Changes in Forcing, *J Adv Model Earth Sy*, 12, 2020.
- Collier, N., Hoffman, F. M., Lawrence, D. M., Keppel-Aleks, G., Koven, C. D., Riley, W. J., Mu, M. Q., and Randerson, J. T.: The International Land Model Benchmarking (ILAMB) System: Design, Theory, and Implementation, *J Adv Model Earth Sy*, 10, 2731-2754, 2018.
- 25 Davies-Barnard, T., Meyerholt, J., Zaehle, S., Friedlingstein, P., Brovkin, V., Fan, Y. C., Fisher, R. A., Jones, C. D., Lee, H., Peano, D., Smith, B., Warlind, D., and Wiltshire, A. J.: Nitrogen cycling in CMIP6 land surface models: progress and limitations, *Biogeosciences*, 17, 5129-5148, 2020.
- Dwivedi, D., Riley, W. J., Torn, M. S., Spycher, N., Maggi, F., and Tang, J. Y.: Mineral properties, microbes, transport, and plant-input profiles control vertical distribution and age of soil carbon stocks, *Soil Biol Biochem*, 107, 244-259, 2017.
- 30 Fisher, R. A. and Koven, C. D.: Perspectives on the Future of Land Surface Models and the Challenges of Representing Complex Terrestrial Systems, *J Adv Model Earth Sy*, 12, 2020.
- Golaz, J. C., Caldwell, P. M., Van Roekel, L. P., Petersen, M. R., Tang, Q., Wolfe, J. D., Abeshu, G., Anantharaj, V., Asay-Davis, X. S., Bader, D. C., Baldwin, S. A., Bisht, G., Bogenschutz, P. A., 35 Branstetter, M., Brunke, M. A., Brus, S. R., Burrows, S. M., Cameron-Smith, P. J., Donahue, A. S., Deakin, M., Easter, R. C., Evans, K. J., Feng, Y., Flanner, M., Foucar, J. G., Fyke, J. G., Griffin, B. M., Hannay, C., Harrop, B. E., Hoffman, M. J., Hunke, E. C., Jacob, R. L., Jacobsen, D. W., Jeffery, N.,



- Jones, P. W., Keen, N. D., Klein, S. A., Larson, V. E., Leung, L. R., Li, H. Y., Lin, W. Y., Lipscomb, W. H., Ma, P. L., Mahajan, S., Maltrud, M. E., Marnett, A., McClean, J. L., McCoy, R. B., Neale, R. B., Price, S. F., Qian, Y., Rasch, P. J., Eyre, J. E. J. R., Riley, W. J., Ringler, T. D., Roberts, A. F., Roesler, E. L., Salinger, A. G., Shaheen, Z., Shi, X. Y., Singh, B., Tang, J. Y., Taylor, M. A., Thornton, P. E.,
5 Turner, A. K., Veneziani, M., Wan, H., Wang, H. L., Wang, S. L., Williams, D. N., Wolfram, P. J.,
Worley, P. H., Xie, S. C., Yang, Y., Yoon, J. H., Zelinka, M. D., Zender, C. S., Zeng, X. B., Zhang, C.
Z., Zhang, K., Zhang, Y., Zheng, X., Zhou, T., and Zhu, Q.: The DOE E3SM Coupled Model Version 1:
Overview and Evaluation at Standard Resolution, *J Adv Model Earth Sy*, 11, 2089-2129, 2019.
- Grant, R. F.: Modelling changes in nitrogen cycling to sustain increases in forest productivity under
10 elevated atmospheric CO₂ and contrasting site conditions, *Biogeosciences*, 10, 7703-7721, 2013.
- Gross, M., Wan, H., Rasch, P. J., Caldwell, P. M., Williamson, D. L., Klocke, D., Jablonowski, C.,
Thatcher, D. R., Wood, N., Cullen, M., Beare, B., Willett, M., Lemarie, F., Blayo, E., Malardel, S.,
Termonia, P., Gassmann, A., Lauritzen, P. H., Johansen, H., Zarzycki, C. M., Sakaguchi, K., and Leung,
R.: Physics-Dynamics Coupling in Weather, Climate, and Earth System Models: Challenges and Recent
15 Progress, *Mon Weather Rev*, 146, 3505-3544, 2018.
- Hirano, T., Kim, H., and Tanaka, Y.: Long-term half-hourly measurement of soil CO₂ concentration and
soil respiration in a temperate deciduous forest, *J Geophys Res-Atmos*, 108, 2003.
- Hoffman, F. M., Randerson, J. T., Arora, V. K., Bao, Q., Cadule, P., Ji, D., Jones, C. D., Kawamiya, M.,
Khatriwala, S., Lindsay, K., Obata, A., Shevliakova, E., Six, K. D., Tjiputra, J. F., Volodin, E. M., and
20 Wu, T.: Causes and implications of persistent atmospheric carbon dioxide biases in Earth System Models,
J Geophys Res-Bioge, 119, 141-162, 2014.
- Huntzinger, D. N., Michalak, A. M., Schwalm, C., Ciais, P., King, A. W., Fang, Y., Schaefer, K., Wei,
Y., Cook, R. B., Fisher, J. B., Hayes, D., Huang, M., Ito, A., Jain, A. K., Lei, H., Lu, C., Maignan, F.,
Mao, J., Parazoo, N., Peng, S., Poulter, B., Ricciuto, D., Shi, X., Tian, H., Wang, W., Zeng, N., and Zhao,
25 F.: Uncertainty in the response of terrestrial carbon sink to environmental drivers undermines carbon-
climate feedback predictions, *Sci Rep-Uk*, 7, 2017.
- Hurrell, J. W., Holland, M. M., Gent, P. R., Ghan, S., Kay, J. E., Kushner, P. J., Lamarque, J. F., Large,
W. G., Lawrence, D., Lindsay, K., Lipscomb, W. H., Long, M. C., Mahowald, N., Marsh, D. R., Neale,
R. B., Rasch, P., Vavrus, S., Vertenstein, M., Bader, D., Collins, W. D., Hack, J. J., Kiehl, J., and Marshall,
30 S.: The Community Earth System Model A Framework for Collaborative Research, *B Am Meteorol Soc*,
94, 1339-1360, 2013.
- Jarvis, N. J., Taylor, A., Larsbo, M., Etana, A., and Rosen, K.: Modelling the effects of bioturbation on
the re-distribution of ¹³⁷Cs in an undisturbed grassland soil, *Eur J Soil Sci*, 61, 24-34, 2010.
- Jung, M., Reichstein, M., Schwalm, C. R., Huntingford, C., Sitch, S., Ahlstrom, A., Arneeth, A., Camps-
35 Valls, G., Ciais, P., Friedlingstein, P., Gans, F., Ichii, K., Ain, A. K. J., Kato, E., Papale, D., Poulter, B.,
Raduly, B., Rodenbeck, C., Tramontana, G., Viovy, N., Wang, Y. P., Weber, U., Zaehle, S., and Zeng,
N.: Compensatory water effects link yearly global land CO₂ sink changes to temperature, *Nature*, 541,
516-520, 2017.
- Koven, C., Friedlingstein, P., Ciais, P., Khvorostyanov, D., Krinner, G., and Tarnocai, C.: On the
40 formation of high-latitude soil carbon stocks: Effects of cryoturbation and insulation by organic matter in
a land surface model, *Geophys Res Lett*, 36, 2009.



- Koven, C. D., Riley, W. J., Subin, Z. M., Tang, J. Y., Torn, M. S., Collins, W. D., Bonan, G. B., Lawrence, D. M., and Swenson, S. C.: The effect of vertically resolved soil biogeochemistry and alternate soil C and N models on C dynamics of CLM4, *Biogeosciences*, 10, 7109-7131, 2013.
- 5 Kumar, A., Jaiswal, D. K., and Kumar, N.: Analytical solutions of one-dimensional advection-diffusion equation with variable coefficients in a finite domain, *J Earth Syst Sci*, 118, 539-549, 2009.
- Le Quere, C., Andrew, R. M., Canadell, J. G., Sitch, S., Korsbakken, J. I., Peters, G. P., Manning, A. C., Boden, T. A., Tans, P. P., Houghton, R. A., Keeling, R. F., Alin, S., Andrews, O. D., Anthoni, P., Barbero, L., Bopp, L., Chevallier, F., Chini, L. P., Ciais, P., Currie, K., Delire, C., Doney, S. C., Friedlingstein, P., Gkritzalis, T., Harris, I., Hauck, J., Haverd, V., Hoppema, M., Goldewijk, K. K., Jain, A. K., Kato, E.,
- 10 Kortzinger, A., Landschutzer, P., Lefevre, N., Lenton, A., Lienert, S., Lombardozzi, D., Melton, J. R., Metzl, N., Millero, F., Monteiro, P. M. S., Munro, D. R., Nabel, J. E. M. S., Nakaoka, S., O'Brien, K., Olsen, A., Omar, A. M., Ono, T., Pierrot, D., Poulter, B., Rodenbeck, C., Salisbury, J., Schuster, U., Schwinger, J., Seferian, R., Skjelvan, I., Stocker, B. D., Sutton, A. J., Takahashi, T., Tian, H. Q., Tilbrook, B., van der Laan-Luijkx, I. T., van der Werf, G. R., Viovy, N., Walker, A. P., Wiltshire, A. J., and Zaehle, S.: Global Carbon Budget 2016, *Earth Syst Sci Data*, 8, 605-649, 2016.
- 15 Luo, Y. Q., Randerson, J. T., Abramowitz, G., Bacour, C., Blyth, E., Carvalhais, N., Ciais, P., Dalmonech, D., Fisher, J. B., Fisher, R., Friedlingstein, P., Hibbard, K., Hoffman, F., Huntzinger, D., Jones, C. D., Koven, C., Lawrence, D., Li, D. J., Mahecha, M., Niu, S. L., Norby, R., Piao, S. L., Qi, X., Peylin, P., Prentice, I. C., Riley, W., Reichstein, M., Schwalm, C., Wang, Y. P., Xia, J. Y., Zaehle, S., and Zhou, X.
- 20 H.: A framework for benchmarking land models, *Biogeosciences*, 9, 3857-3874, 2012.
- Manson, J. R. and Wallis, S. G.: A conservative, semi-Lagrangian fate and transport model for fluvial systems - I. Theoretical development, *Water Res*, 34, 3769-3777, 2000.
- Medvigy, D., Wang, G. S., Zhu, Q., Riley, W. J., Trierweiler, A. M., Waring, B. G., Xu, X. T., and Powers, J. S.: Observed variation in soil properties can drive large variation in modelled forest functioning and composition during tropical forest secondary succession, *New Phytol*, 223, 1820-1833, 2019.
- 25 Munhoven, G.: Model of Early Diagenesis in the Upper Sediment with Adaptable complexity - MEDUSA (v. 2): a time-dependent biogeochemical sediment module for Earth system models, process analysis and teaching, *Geosci Model Dev*, 14, 3603-3631, 2021.
- Oleson, K. W., Lawrence, D. M., Bonan, G. B., Drewniak, B., Huang, M., Koven, C. D., Levis, S., Li, F.,
- 30 Riley, W. J., Subin, Z. M., Swenson, S. C., Thornton, P. E., Bozbiyik, A., Fisher, R., Heald, C. L., Kluzek, E., Lamarque, J. F., Lawrence, P. J., Leung, L. R., Lipscomb, W. H., Muszala, S., Ricciuto, D. M., Sacks, W., Sun, Y., Tang, J. Y., and Yang, Z.: Technical Description of version 4.5 of the Community Land Model (CLM), National Center for Atmospheric Research, Boulder, Colorado, 2013.
- Petrovskii, S. and Petrovskaya, N.: Computational ecology as an emerging science, *Interface Focus*, 2, 241-254, 2012.
- 35 Riley, W. J., Sierra, C., Tang, J. Y., Bouskill, N. J., Zhu, Q., and Abramoff, R.: Next generation soil biogeochemistry model representations: A proposed community open source model farm (BeTR-S) In: *Multi-scale Biogeochemical Processes in Soil Ecosystems: Critical Reactions and Resilience to Climate Changes*, Yang, Y., Keiluweit, M., Senesi, N., and Xing, B. (Eds.), 2021.
- 40 Riley, W. J., Zhu, Q., and Tang, J. Y.: Weaker land-climate feedbacks from nutrient uptake during photosynthesis-inactive periods, *Nat Clim Change*, 8, 1002-1006, 2018.



- Simpson, M. J. and Landman, K. A.: Analysis of split operator methods applied to reactive transport with Monod kinetics, *Adv Water Resour*, 30, 2026-2033, 2007.
- Tang, J., Zhuang, Q., Shannon, R. D., and White, J. R.: Quantifying wetland methane emissions with process-based models of different complexities, *Biogeosciences*, 7, 3817-3837, 2010.
- 5 Tang, J. Y. and Riley, W. J.: Linear two-pool models are insufficient to infer soil organic matter decomposition temperature sensitivity from incubations, *Biogeochemistry*, 149, 251-261, 2020.
- Tang, J. Y. and Riley, W. J.: On the modeling paradigm of plant root nutrient acquisition, *Plant Soil*, 459, 441-451, 2021.
- Tang, J. Y. and Riley, W. J.: Predicted Land Carbon Dynamics Are Strongly Dependent on the Numerical
10 Coupling of Nitrogen Mobilizing and Immobilizing Processes: A Demonstration with the E3SM Land Model, *Earth Interact*, 22, 2018.
- Tang, J. Y. and Riley, W. J.: Technical Note: A generic law-of-the-minimum flux limiter for simulating substrate limitation in biogeochemical models, *Biogeosciences*, 13, 723-735, 2016.
- Tang, J. Y. and Riley, W. J.: Technical Note: Simple formulations and solutions of the dual-phase
15 diffusive transport for biogeochemical modeling, *Biogeosciences*, 11, 3721-3728, 2014.
- Tang, J. Y. and Riley, W. J.: A total quasi-steady-state formulation of substrate uptake kinetics in complex networks and an example application to microbial litter decomposition, *Biogeosciences*, 10, 8329-8351, 2013.
- Tang, J. Y., Riley, W. J., Koven, C. D., and Subin, Z. M.: CLM4-BeTR, a generic biogeochemical
20 transport and reaction module for CLM4: model development, evaluation, and application, *Geosci Model Dev*, 6, 127-140, 2013.
- Todd-Brown, K. E. O., Randerson, J. T., Hopkins, F., Arora, V., Hajima, T., Jones, C., Shevliakova, E., Tjiputra, J., Volodin, E., Wu, T., Zhang, Q., and Allison, S. D.: Changes in soil organic carbon storage predicted by Earth system models during the 21st century, *Biogeosciences*, 11, 2341-2356, 2014.
- 25 Tramontana, G., Jung, M., Schwalm, C. R., Ichii, K., Camps-Valls, G., Raduly, B., Reichstein, M., Arain, M. A., Cescatti, A., Kiely, G., Merbold, L., Serrano-Ortiz, P., Sickert, S., Wolf, S., and Papale, D.: Predicting carbon dioxide and energy fluxes across global FLUXNET sites with regression algorithms, *Biogeosciences*, 13, 4291-4313, 2016.
- Wieder, W. R., Allison, S. D., Davidson, E. A., Georgiou, K., Hararuk, O., He, Y. J., Hopkins, F., Luo, Y. Q., Smith, M. J., Sulman, B., Todd-Brown, K., Wang, Y. P., Xia, J. Y., and Xu, X. F.: Explicitly
30 representing soil microbial processes in Earth system models, *Global Biogeochem Cy*, 29, 1782-1800, 2015.
- Zaehle, S., Medlyn, B. E., De Kauwe, M. G., Walker, A. P., Dietze, M. C., Hickler, T., Luo, Y. Q., Wang, Y. P., El-Masri, B., Thornton, P., Jain, A., Wang, S. S., Warlind, D., Weng, E. S., Parton, W., Iversen, C.
35 M., Gallet-Budynek, A., McCarthy, H., Finzi, A. C., Hanson, P. J., Prentice, I. C., Oren, R., and Norby, R. J.: Evaluation of 11 terrestrial carbon-nitrogen cycle models against observations from two temperate Free-Air CO₂ Enrichment studies, *New Phytol*, 202, 803-822, 2014.
- Zhu, Q., Riley, W. J., Tang, J., and Koven, C. D.: Multiple soil nutrient competition between plants, microbes, and mineral surfaces: model development, parameterization, and example applications in
40 several tropical forests, *Biogeosciences*, 13, 341-363, 2016.
- Zhu, Q., Riley, W. J., and Tang, J. Y.: A new theory of plant-microbe nutrient competition resolves inconsistencies between observations and model predictions, *Ecol Appl*, 27, 875-886, 2017.



Zhu, Q., Riley, W. J., Tang, J. Y., Collier, N., Hoffman, F. M., Yang, X. J., and Bisht, G.: Representing nitrogen, phosphorus, and carbon interactions in the E3SM land model: development and dlobal benchmarking, *J Adv Model Earth Sy*, 11, 2238-2258, 2019.